Soft Matter

Accepted Manuscript

ROYAL SOCIETY OF CHEMISTRY

www.rsc.org/softmatter

Orientation, interaction and laser assisted self-assembly of organic single-crystal micro-sheets in nematic liquid crystal

M. V. Rasna[1], K. P. Zuhail[1], U. V. Ramudu[2], R. Chandrasekar[2] J. Dontabhaktunia[3] and Surajit Dhara[1*]

[1]*School of Physics, University of Hyderabad, Hyderabad-500046, India*
[2]*School of Chemistry, University of Hyderabad, Hyderabad-500046, India*
[3] *School of Natural Sciences, Mahindra Ecole Centrale, Hyderabad-500043, India*

(Dated: August 10, 2015)

Colloidal self-assembly has been one of the major driving themes in material science to obtain functional and advanced optical materials with complex architecture. Most of the nematic colloids reported so far are based on the optically isotropic spherical microparticles. We study organic single crystal micro-sheets and investigate their orientation, interaction and directed assembly in a nematic liquid crystal. The micro-sheets induce planar surface anchoring of the liquid crystal. The elasticity mediated pair interaction of micro-sheets shows quadrupolar characteristics. The average orientation angle of the micro-sheets in planar cell and the angle between two micro-sheets in homeotropic cell are supported by the Landau-de Gennes Q-tensor modeling. The self-assembly of the micro-sheets are assisted by laser tweezer to form larger two-dimensional structure which are potential for photonics applications of colloids.

I. INTRODUCTION

Nematic colloids prepared by dispersing micrometer sized colloidal particles in nematic liquid crystals (LCs) received considerable attention due to its potential application in the field of soft materials and photonics [1–7]. The inclusion of foreign particles disturbs the uniform director field (average direction of molecular alignment) and induce point or line defects and the corresponding elastic distortion spreads over a few micrometer range [8–14]. The defect formation is due to the competition between the bulk elastic property of the medium and the anchoring of LC molecules on the particle's surface. In case of normal surface anchoring, each spherical microparticle forms a source of singularity (radial hedgehog defect) and for the conservation of topological charge, a hyperbolic hedgehog defect appears in the director field and known as elastic dipoles [14]. For weak anchoring the defect appears in the form of a thin disclination line encircling the colloidal particles (Saturn ring) and known as quadrupoles [14]. Similarly with planar surface anchoring, the microspheres induce two surface point defects at the poles along the director and are known as boojums [14, 16]. The interaction among these colloids are mediated by sharing the topological defects and there are many theoretical and experimental reports on the colloidal interactions in nematic liquid crystals [1, 2, 8–13]. Colloidal self-assembly mediated by the nematic elasticity are potential for photonic applications such as photonic band gap crystals, metamaterials, 3D photonic crystals [17–21].

Most of the reports on nematic colloids are concerned on the inclusion of spherical microparticles. In the recent years significant interest is observed on the dispersion of nonspherical microparticles such as rod-shaped,

star-shaped, triangular, square, bullet and doughnut shaped in nematic liquid crystals [23–33]. Lapointe et al., showed that polygonal platelets exhibit either dipolar or quadrupolar interactions in nematic liquid crystal depending on whether the platelets have an odd or even number of sides [25]. Very recently it has been shown by computer simulation that quasicrystalline colloidal lattices can be achieved in nematic liquid crystal using pentagonal colloidal platelets [22]. In previous experiments, the microparticles used were either silica or made of amorphous materials, which were optically isotropic. In this paper we report on the orientation, interactions and laser assisted self-assembly of organic single crystal micro-sheets in a nematic liquid crystal.

II. EXPERIMENT

Micro-sheets were prepared as per the reported procedure [34]. It grows either in rectangular or hexagonal shape. Typical size of the rectangular platelets i.e., lengths and widths are in the range of 9 to 10 μm and 4 to 5 μm respectively. The average thickness of the platelets is about 200nm. The micro-sheets have monoclinic crystal structure and are optically birefringent ($\Delta n = 0.25 \pm 0.05$). It emits fluorescence bands at 515 and 653 nm upon excitation of 431 nm. It can be used as organic waveguides and wavelength filters at different wavelengths [34]. The platelets are dispersed in 5CB (pentyl cyanobiphenyl) liquid crystal by physical mixing. The experimental cells with various spacing were fabricated using glass plates that are spin coated with polyimide AL-1254 and cured at 180°C for 1h. They were rubbed antiparallel way for homogeneous alignment of the nematic director. For homeotropic cells, we used polyimide JALS-204 and cured at 200°C for 1h. A laser tweezer was built on an inverted microscope (Nikon eclipse Ti-U) using a CW diode-pumped solid state laser operating at 1064 nm. The trajectory of the particle are

---

* sdsp@uohyd.ernet.in

video recorded with CCD camera (Pixelink PLB 741F) and appropriate computer program was used to track the centers of the micro-sheets.

III. NUMERICAL MODELLING

We employed Landau-de Gennes phenomenological theory to model our experimental system [35]. Free energy of the system constitutes contributions from elasticity of the nematic medium, temperature dependent bulk order and the surface anchoring. It is written in terms of tensorial order parameter Q_{ij}:

$$f = \frac{1}{2}L(\partial Q_{ij}/\partial x_k)^2 + \frac{1}{2}AQ_{ij}Q_{ji} + \frac{1}{3}BQ_{ij}Q_{jk}Q_{ki}$$
$$+ \frac{1}{4}C(Q_{ij}Q_{ij})^2 + f_S \quad (1)$$

The contribution from surface of the platelets inducing degenerate planar anchoring is given by $f_S = W(\widetilde{Q}_{ij} - \widetilde{Q}_{ij}^{\perp})^2$, where W is the anchoring strength, while the term $\widetilde{Q}_{ij} - \widetilde{Q}_{ij}^{\perp}$ imposes the orientational in-plane ordering. Free energy is minimized using explicit finite difference relaxation method on a cubic mesh. Rectangular micro-sheets of length $l = 360nm$ and breadth $b = 180nm$ are considered for simulations in a micron thick liquid crystal cell maintaining the same aspect ratios as that of the experiments. Degenerate planar surface anchoring of strength $W = 10^{-3}J/m^2$ is induced by all the surfaces of the microsheets. Top and bottom substrates of the liquid crystal cell induce strong uniform planar anchoring in the case of planar cell and periodic boundary conditions are assumed along XY directions. In the case of homeotropic cell, the top and bottom substrates induce strong homeotropic anchoring of strength $W = 10^{-3}J/m^2$. All the material parameters considered in the simulations are that of a standard nematic liquid crystal [35].

IV. RESULTS AND DISCUSSION

Figure 1(a) shows the optical microscope image of a large number of micro-sheets on the glass slide. Figure 1(b) and (c) shows the polarising microscope images of a rectangular micro-sheet at two different orientations. It is clearly observed that the micro-sheets are optically anisotropic and the optical axis is either parallel or perpendicular to the long axis. Figure 2(a) shows the image of a few micro-sheets dispersed in 5CB liquid crystal in a planar cell. It is observed that the long axes of the micro-sheets are making some angle with respect to the rubbing direction. Figure 2(b) shows the fluorescence image of the micro-sheets when illuminated with blue filter. The wavelength of the red colour is 653 nm. Figure 2(c) shows the histogram of the angles of long axes (θ) with respect to the rubbing direction. The maximum number of
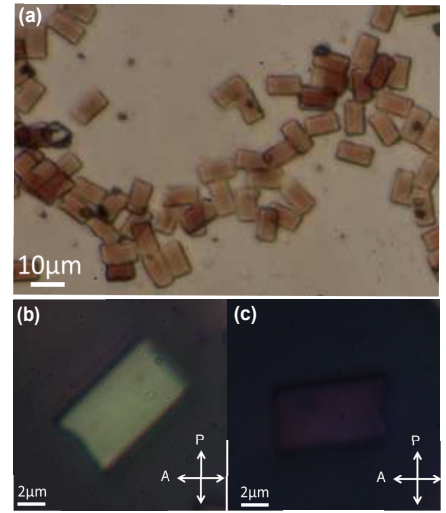
FIG. 1. (a) Optical microscope image of rectangular single crystal micro-sheets. Polarised optical microscope images of a micro-sheet with the long axis (b) making 45° with respect to the polariser and (c) parallel to the polariser.
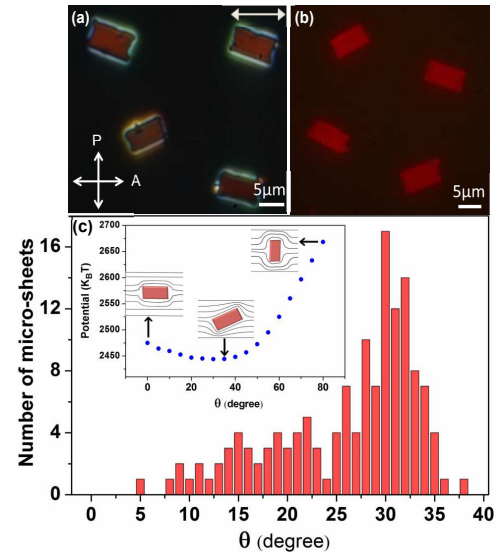
FIG. 2. (a) Platelets dispersed in aligned nematic liquid crystal. The white arrow at the right corner indicates the rubbing direction (optical axis of LC). (b) Fluorescence image the platelets illuminated with blue filter. (c) Distribution of angles of the long axes of the platelets with respect to rubbing direction. (Inset) Variation of free energy of a microsheet for various in-plane rotations.

particles are orientated making about 33° with respect the rubbing direction. Using Landau de-gennes Q-tensor modelling we calculated free energy for various in-plane orientations. The variation of free energy with θ is shown in the inset of Fig.2(c). It is observed that the energy is minimum at $\theta \simeq 35°$ which is very close to the average orientation angle of the rectangular micro-sheets. The wide distribution of θ in Fig.2(c) could be due to the

non-uniformity in size, shape and edge roughness of the micro-sheets.

To understand the molecular orientation of the liquid crystal around the micro-sheet, images were taken between crossed polarisers with a λ-plate (red-plate) inserted between the sample and the polariser. Figure 3(a) shows the red-plate image of a micro-sheet. The plane of the micro-sheet is parallel to the substrate surface. The bluish and yellowish colors around the micro-sheet correspond to the clockwise and anti-clockwise rotation of the director from the rubbing direction. It indicates the planar anchoring of the director on the surface of the micro-sheet. The strongest distortion of nematic are at the edges and the corners. Experimentally, it is difficult to precisely locate the defects on the micro-sheets. The calculated director field surrounding the micro-particle is shown by head-less vectors in Fig.3(b). The director profile apparently have well-defined winding numbers reminiscent to $+1/2$ and $-1/2$ defect lines similar to that was reported in case of square-shaped particles [4]. In case of rectangular micro-sheets, there is an asymmetry about the y-direction (perpendicular to the rubbing direction) which is evident from the simulated director profile and indicated by red-lines. Figure 3(c) shows the image of a micro-sheet in a homeotropic cell. The plane of the micro-sheet is vertical with respect to the substrate surfaces. The brighter edges in Fig.3(c) indicate that the long axis of the micro-sheet is tilted with respect to the vertical direction. The variation of calculated free energy of a micro-particle in a homeotropic cell at various tilt angles with respect to the z-axis (normal to the cell substrate) is shown in Fig.3(d). It is observed that the minimum energy is obtained at an angle of 22°.
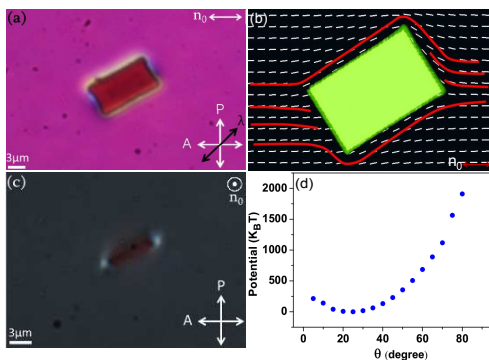
FIG. 3. (Color online) (a) Polarising optical microscope image of a micro-sheet with a red-plate (λ-plate, 530nm) in a planar cell. Cell thickness 12 μm. The direction of λ-plate is shown with a black arrow. (b) The calculated director field surrounding the micro-particles is shown as head-less vectors in white. The red lines indicates the asymmetry of the director field. (c) A micro-sheet in a homeotropic cell (d) Variation of free energy at various title angles with respect to the z-axis. Cell thickness 15 μm.

The interaction between two micro-sheets is studied by video microscopy technique. In order to measure the elas-

tic interaction, the viscus drag coefficient of the micro-sheets is calculated. The drag coefficients are determined directly from the study of Brownian motion of the micro-sheets in the liquid crystal [25, 36]. In a homogeneous cell, the Brownian motion of a preselected micro-sheet which is far away from the other micro-sheets is video recorded and the trajectory of the micro-sheet is determined from the particle tracking. Figure 4 shows the typical histograms of displacement parallel and perpendicular to the director ($\mathbf{n}$) obtained from the trajectory for a time delay $\tau=$ 0.05 sec. The histograms of the displacement along (x-axis) and perpendicular to the director (y-axis) show the anisotropy in the motion. Here the x-displacement is shifted along the positive x direction, which indicate macroscopic flow. Similar behavior was also reported by Tkalec *et al.,* in case of micro-rod dispersed in nematic liquid crystals [23]. The mean square displacement along the perpendicular ($\sigma_\perp^2$) and parallel ($\sigma_\parallel^2$) to the director varies linearly with τ and the slope of the linear fits give the respective diffusion coefficients ($D_\parallel$ and $D_\perp$). At room temperature, from the linear fit, we get $D_\parallel = 6.2 \times 10^{-3} \mu m^2$/sec and $D_\perp = 4.5 \times 10^{-3} \mu m^2$/sec. The drag coefficients are calculated from the Einstein relation, $\zeta_i = k_B T/D_i$, where the subscript i stands for $\parallel$ or $\perp$ to the director. At T= 298K we get, $\zeta_\parallel = 0.66 \times 10^{-6}$ kg/sec and $\zeta_\perp = 0.92 \times 10^{-6}$ kg/sec.
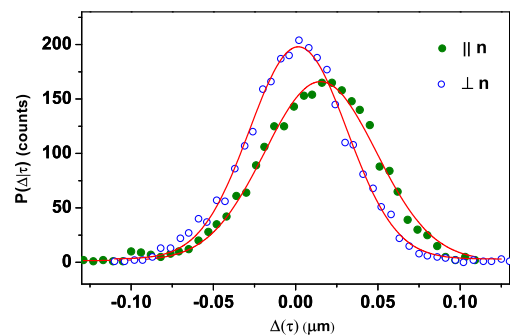
FIG. 4. (Color online)(a) Histograms of displacement along the parallel and the perpendicular to the director obtained from the trajectory for time delay τ=0.05 sec. The red lines are the Gaussian fits to the data. Note that the histogram is displaced along positive x-direction due to the macroscopic flow.

The elastic force is balanced by the viscus drag force in the nematic media which is given by $F_{drag} = -\zeta dR(t)/dt$, where $dR(t)/dt$ is the time derivative of inter-particle separation. When the elastic force (F_{el}) is balanced by viscus drag force, the equation of motion is given by, $F_{el} + F_{drag}=0$. The micro-sheets have quadrupolar interaction and the corresponding force is given by $F_{el} = -k/R^6$, where k is a constant that depends on the mean elastic constant K, geometry and the size of the micro-sheet. The time dependent particle separation is given by $R(t) = (R_0^7 - 7\alpha t)^{1/7}$, where $\alpha = k/\zeta$ and R_0 is the initial separation at time $t = 0$. The strength
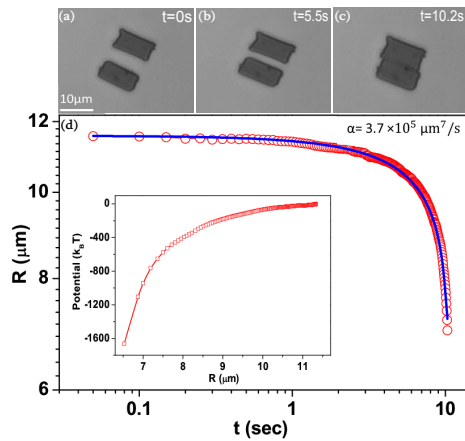
FIG. 5. (Color online) Elastic interaction of the micro-sheets along the broad-side on position. (a)-(c) Sequence of CCD images of the micro-sheets taken at different times. (d) Variation of inter-particle separation ($R(t)$) with time (logarithmic scale). Blue line shows the nonlinear least square fit to $R(t) = (R_0^7\text{-}7\alpha t)^{1/7}$. (Inset) The elastic interaction potential as a function of separation.

of elastic interaction between the micro-sheets are studied by positioning two micro-sheets in the defined locations namely along the broadside-on (Fig.5(a)) and end-on (Fig.6(a)) positions by using the laser tweezer. After removing the laser power the trajectories of the micro-sheets are video recorded and their time dependent position is determined by particle tracking. The instantaneous force on the particle is calculated from the numerical differentiation of the trajectory and the interaction potential is calculated by integrating the force over the distance travelled.
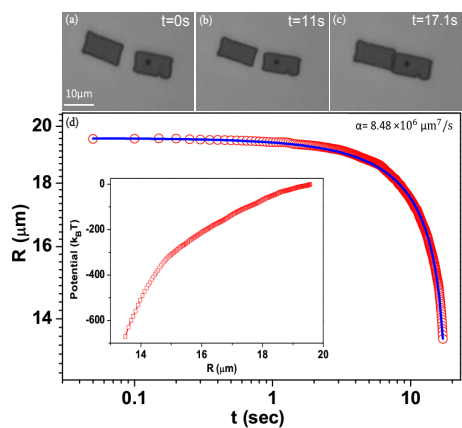
FIG. 6. (Color online)Elastic interaction of the micro-sheets along the end-on position. (a)-(c) Sequence of CCD images of the micro-sheets taken at different times. (d) Variation of inter-particle separation ($R(t)$) with time (logarithmic scale). Blue line shows the nonlinear least square fit to $R(t) = (R_0^7\text{-}7\alpha t)^{1/7}$. (Inset) the elastic interaction potential as a function of separation.

Figure 5(d) shows the inter-particle separation ($R(t)$) of the micro-sheets along the broadside-on position. The least square fit provides $\alpha = 3.7\times10^5$ $\mu\text{m}^7/\text{sec}$. A few CCD images at different times are also shown in Fig.5. Using this value of α and the drag coefficients the calculated maximum attractive force for separation $R = 6.5\mu m$ is 4pN. The inset of Fig.5(d) shows the elastic interaction potential obtained by integrating the force ($U = \int F_{drag}.dR$) as a function of separation R. The lowest potential energy is about $-1600k_B$T. Figure 6(d) shows the time variation of inter-particle separation of the micro-sheets along the end-on position. The maximum attractive force for the separation $R = 13.4\mu m$ is 1.2 pN. The inset of Fig.6(d) shows the variation of interaction potential as a function of R. The lowest potential obtained in this position is about $-700k_B$T. We observe that the interaction potential along the broadside-on position is relatively stronger than that of the end-on position. Similar behavior was observed in case of micro-rods with homeotropic surface anchoring dispersed in nematic liquid crystal [23]. This is due to the larger reduction of elastic distortion associated with the broadside-on position of the micro-sheets.
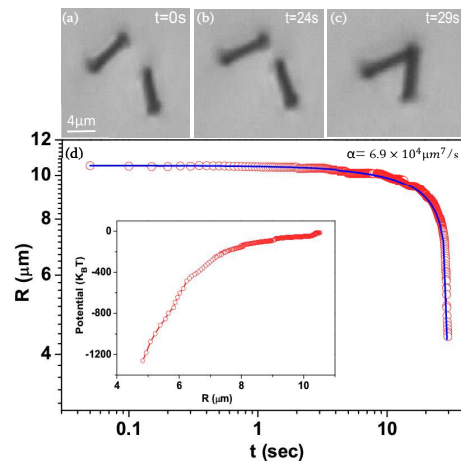
FIG. 7. (Color online) Elastic interaction of the micro-sheets in homeotropic cell. (a)-(c) Sequence of CCD images of the micro-sheets taken at different times. The angle between two micro-sheets in (c) is about 60°. (d) Variation of inter-particle separation ($R(t)$) with time (logarithmic scale). Blue line shows the nonlinear least square fit to $R(t) = (R_0^7\text{-}7\alpha t)^{1/7}$. (Inset) the elastic interaction potential as a function of separation.

We also studied the interaction between two micro-sheets in a homeotropic cell. A few CCD images at different times are also shown in Fig.7(a)-(c). Fig. 7(d) shows the inter-particle separation ($R(t)$) of the micro-sheets with time. The least square fit provides $\alpha = 4.8\times10^5$ $\mu\text{m}^7/\text{sec}$ and the calculated maximum attractive force for separation $R = 4.8\mu m$ is 3.8pN. The inset of Fig.7(d) shows the variation of elastic interaction potential as a function of separation R. The lowest potential energy is about $-1200k_B$T. We observe that the

equilibrium angle between the two micro-sheets varies within 55 to 60° (Fig.7(c)). We numerically calculated the interaction between two micro-sheets. In simulations the sheets are kept at a fixed distance with their smaller edges parallel to the plane of the substrate and the interaction potential is calculated by varying the mutual angle (see Fig.8). The angle is zero when both the sheets are parallel to each other with their large surfaces facing towards one another. The nematic distortions around the micro-sheets control the angle between them. As the angle increases, the distortions reduce and the sheets stabilise at 55° to each other.
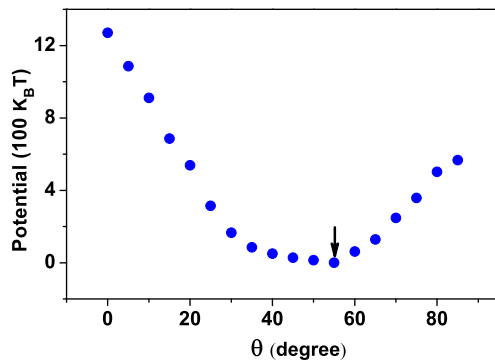
FIG. 8. (Color online) Variation of potential energy with angle between the two micro-sheets in homeotropic cell. The minima of the free energy is marked with a downward arrow.
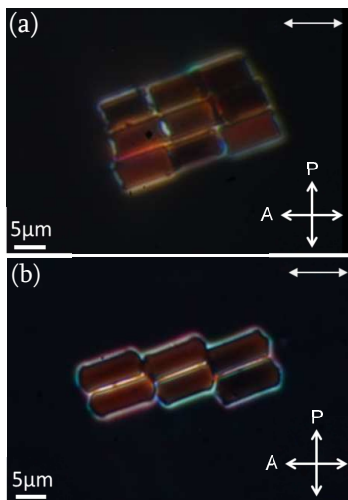
FIG. 9. (Color online) Polarising optical microscope images of laser assisted self-assembly of (a) rectangular and (b) hexagonal micro-sheets in 5CB liquid crystal. The double headed white arrows at the right corners show the far field alignment of the director.

The micro-sheets have inherent tendency to self-

assemble due to the topological defect mediated long-range attractive interactions as discussed. We used the laser tweezer to assist the self-assembly of the micro-sheets to form a larger crystal. For the purpose of demonstration of this idea, we show the assembly of a few rectangular and hexagonal micro-sheets in Fig.9. It may be mentioned that micro-sheets absorb 431 nm and give two fluorescence band in the red region (653 nm). Here they appear reddish under white light illumination. The slight variation in the intensity of color could be due to different sheet thickness and slight difference in the molecular orientation on the micro-sheets. Thus, the single crystal micro-sheets could be used as building blocks for making larger 2D colloidal crystal. It may be mentioned that the micro-sheets were crystallized in tetrahydrofuran/water (THF/H_2O) solvents. They have some edge roughness as a result there are some voids in the assembled structure (Fig.9(a)). However, it is possible to obtain micro-sheets with smoother edge under controlled condition. Some preliminary experiment shows that the hexagonal micro-sheets have better edge smoothness and consequently the packing is better (Fig.9(b)).

V. CONCLUSIONS

In conclusion, we observed single crystal micro-sheets induce planar anchoring of the nematic liquid crystal and the interaction potential between two micro-particles is quadrupolar and anisotropic. The equilibrium orientation angle of a micro-sheet in planar cell, and angle between two micro-sheets in homeotropic cell are qualitatively in agreement with the Landau de-Gennes Q-tensor modelling. We demonstrated laser assisted 2D self-assembly exploiting the long-range elastic interaction. Our experiment opens up the possibility for making larger organic 2D crystal using micro-sheets as building blocks. The laser assisted self-assembly of micro-sheets with both shape and optical anisotropy could be useful for various optical applications. These particles also show interesting multi-axis rotations under applied electric field, and the details will be reported elsewhere. In addition, the high birefringence of the particles may results in large torque acting to spin and align them in the optical field which can be useful as torque sensors [37, 38].

VI. ACKNOWLEDGEMENT

[1] P. Poulin, H. Stark, T. C. Lubensky and D. A. Weitz, Science **275**, 1770 (1997).

[2] T. C. Lubensky, D. Pettey, N. Currier and H. Stark, Phys. Rev. E **57**, 610 (1998).

[3] I. Musevic, M. Skarabot, U. Tkalec, M. Ravnik and S. Zumer Science **313**, 954 (2006).

[4] J. Dontabhaktuni, M. Ravnik and S. Zumer, Soft Matter **8**, 1657 (2012).

[5] I. Musevic and M. Skarabot, Soft Matter **4**, 195 (2008).

[6] M. Skarabot, M. Ravnik, U. Tkalec, I. Poberaj, D. Babic, N. Osterman and I. Musevic, Phys. Rev. E **76**, 051406 (2007).

[7] K. P. Zuhail, P. Sathyanarayana, D. Sec, S. Copar, M. Skarabot, I. Musevic and S. Dhara, Phys. Rev. E **91**, 030501(R) (2015).

[8] A. Nych, U. Ognysta, M. Skarabot, M. Ravnik, S. Zumer and I. Musevic, Nat. Commun., **4**, 1489 (2013).

[9] O. Guzman, E. B. Kim, S. N. Grollau, L. Abbott and J. J. Pablo, Phys. Rev. Lett., **91**, 235507 (2003).

[10] M. Ravnik, M. Skarabot, S. Zumer, U. Tkalec, I. Poberaj, D. Babic, N. Osterman and I. Musevic, Phys. Rev. Lett., **99**, 247801 (2007).

[11] M. Vilfan, N. Osterman, M. Copic, M. Ravnik, S. Zumer, J. Kotar, D. Babic, I. Poberaj, Phys. Rev. Lett., **101**, 237801 (2008).

[12] T. A. Wood, J. S. Lintuvuori and A. B. Schofield, D. Marenduzzo and W. C. K. Poon, Science **334**, 79 (2011).

[13] K. Takahashi, M. Ichikawa and Y. Kimura, J. Phys. Condens. Matter **20**, 075106 (2008).

[14] H. Stark, Phys. Rep., **351**, 387 (2001).

[15] T. C. Lubensky, D. Petty, N. Currier, and H. Stark, Phys. Rev. E **57**, 610 (1998).

[16] Q. Liu, B. Senyuk, M. Tasinkevych and I. I. Smalyukh, Proc. Natl. Acad. Sci., (USA) **110**, 9231 (2013).

[17] Y. A. Vlasov, X.-Z. Bo, J. C. Sturm and D. J. Norris, Nature **414**, 289 (2001).

[18] J. D. Joannopoulos, P. R. Villeneuve and S. Fan, Nature **386**, 143 (1997).

[19] V. G. Veselago, Sov. Phys. Usp., **10**, 509 (1968).

[20] J. B. Pendry, Phys. Rev. Lett., **85**, 3966 (2000).

[21] K. J. Stebe, E. Lewandowski and M. Ghosh, Science **325**, 159 (2009).

[22] J. Dontabhaktunia, M. Ravnik, and S. Zumer, Proc. Natl. Acad. Sci., (USA) **111**, 2464 (2014).

[23] U. Tkalec, M. Skarabot and I Musevic, Soft Matter **4**, 2402 (2008).

[24] C. P. Lapointe, K. Mayoral and T. G. Mason, Soft Matter **9**, 7843 (2013).

[25] C. P. Lapointe, T. G. Mason and I. I. Smalyukh, Science **326**, 1083 (2009).

[26] M. A. Gharbi, M. Cavallaro, G. Wu, D. A. Beller, R. D. Kamien, S. Yang and K. J. Stebe, Liq. Cryst., **40**, 1619 (2013).

[27] J. S. Evans, C. N. Beier and I. I. Smalyukh, J. Appl. Phys., **110**, 033535 (2011).

[28] D. A. Beller, M. A. Gharbi and I. B. Liu, Soft Matter **11**, 1078 (2015).

[29] A. Martinez, T. Lee, T. Asavei, H. Rubinsztein-Dunlop and I. I. Smalyukh, Soft Matter **8**, 2432 (2012) .

[30] D. Andrienko, M. P. Allen, G. Skacej and S. Zumer, Phys. Rev. E **65**, 041702 (2002).

[31] B. Senyuk, M. C. M. Varney, J. A. Lopez, S.Wang, N. Wu and I. I. Smalyukh, Soft Matter **10**, 6014 (2014).

[32] B. Senyuk, Q. Liu, E. Bililign, P. D. Nystrom and I. I. Smalyukh, Phy. Rev. E **91**, 040501(R) (2015).

[33] B. Senyuk, Q. Liu, S. He, R. D. Kamien, R. B. Kusner, T. C. Lubensky and I. I. Smalyukh, Nature **493**, 200 (2013).

[34] N. Chandrasekhar, S. Basak, M. A. Mohiddon and R. Chandrasekhar. ACS Appl. Mater. Interfaces **6**, 1488 (2014).

[35] M. Ravnik and S Zumar, Liq. Cryst. **36**, 1201 (2009).

[36] S. Dhara, J. Ananthaiah, P. Sathyanarayana, V. Ashok, A. Spadlo and R. Dabrowski, Phys. Rev. E **87**, 030501(R) (2013).

[37] T. A. Nieminen, N. R. Heckenberg, and H. Rubinsztein-Dunlop, J. Mod. Opt. **48**, 405 (2001).

[38] M. E. J. Friese, T. A. Nieminen, N. R. Heckenberg, and H. Rubinsztein-Dunlop, Nature **394**, 348 (1998).